Molecular and Structural Insight into the Role of Key Residues of Thrombospondin-1 and Calreticulin in Thrombospondin-1-Calreticulin Binding

Running Title: Structural bases for the role of key residues of TSP1 and CRT in TSP1-CRT interactions

Qi Yan[1], Joanne E. Murphy-Ullrich[2], Yuhua Song[1*]

[1]Department of Biomedical Engineering, [2]Department of Pathology, The University of Alabama at Birmingham, Birmingham, AL 35294

* To whom correspondence should be addressed:
Department of Biomedical Engineering
The University of Alabama at Birmingham
803 Shelby Interdisciplinary Biomedical Research Building
1825 University Boulevard
Birmingham, AL 35294
Phone: (205) 996-6939 Fax: (205) 975-4919
E-mail: yhsong@uab.edu
Web: http://www.eng.uab.edu/yhsong

† This work was supported by TeraGrid supercomputer allocation (NSF- MCB090009) to Y.H.Song, and NIH HL79644 to J.E.MU.

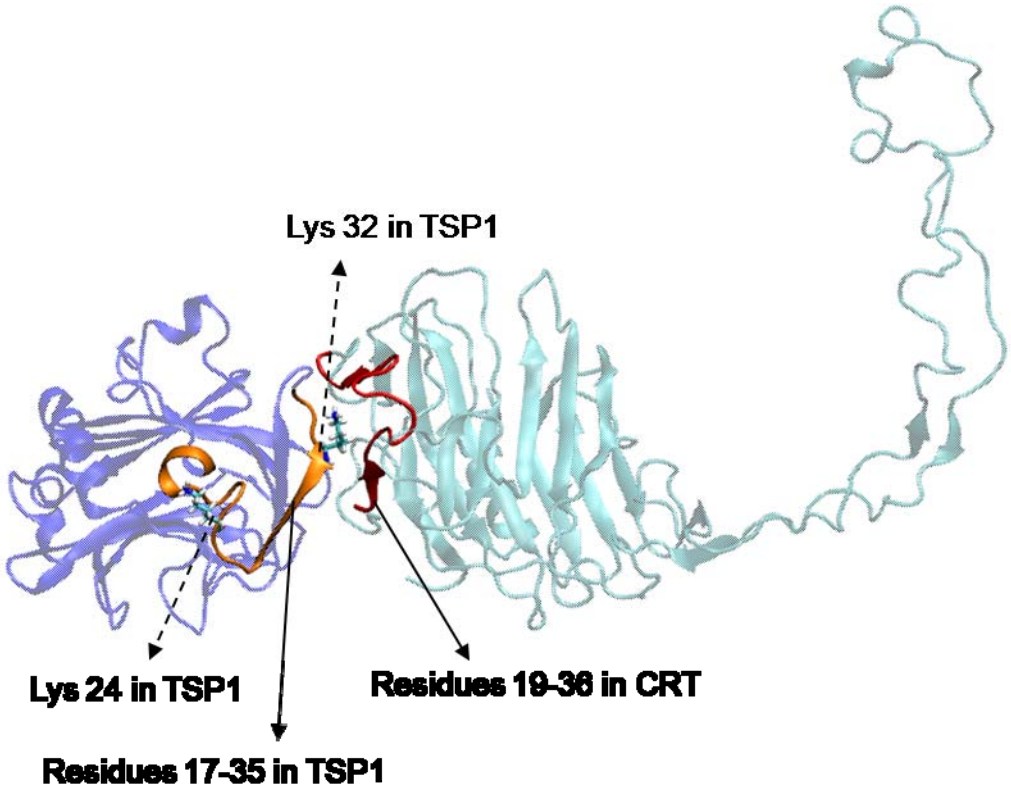

Figure 1S. TSP1-CRT complex. Blue: TSP1; orange: CRT binding site in TSP1 (residues 17-35 in TSP1); cyan: CRT; red: TSP1 binding site in CRT (residues 19-36 in CRT); residues represented with licorice are the key residues of Lys 32 and Lys 24 in TSP1 critical for TSP1-CRT binding (ref. 20). Image was made with VMD software support.

Constant force steered molecular dynamics simulations

We applied the constant external force of 20 pN on the C_a atom of each residue on beta sheets of TSP1 except the residues in CRT binding site. The residues in the structurally stable N-domain and the partial C-domain of CRT, except the residues in the binding site for TSP1, were treated as rigid and were fixed, and leave the structurally flexible P-domain of CRT as unfixed and flexible region. The pulling direction was along the center of the mass of the pulled residues and the fixed residues. 96 residues in TSP1 experienced the external force. The total external

force applied to the TSP1-CRT complex for SMD simulations was 1920 pN. The extension profiles over time in the constant force SMD simulations for the TSP1-CRT complex and its mutants were obtained. The calculated results about the effect of residues 24 and 32 mutations of TSP1 and the mutation of residues 24-26 and 32-34 to Ala in CRT on TSP1-CRT unbinding were compared with experimental results for the validation.

Under the constant force SMD simulations, the extension profile for TSP1-CRT complex, TSP1 K24A&K32A mutant-CRT complex and the TSP1-CRT mutant complex showed that under the same external load pulling, it took longer time for causing the significantly increased distance between the centers of the mass of the binding sites of the TSP1-CRT complex for the wildtype TSP1-CRT complex than its mutants (Fig. 2S). The results showed that TSP1 K24A&K32A mutations in TSP1 and the mutations of amino acids 24-26 and 32-34 in CRT to Ala significantly decreased the binding strength between TSP1 and CRT, which was validated with the experimental results (ref. 3, 7, 16).

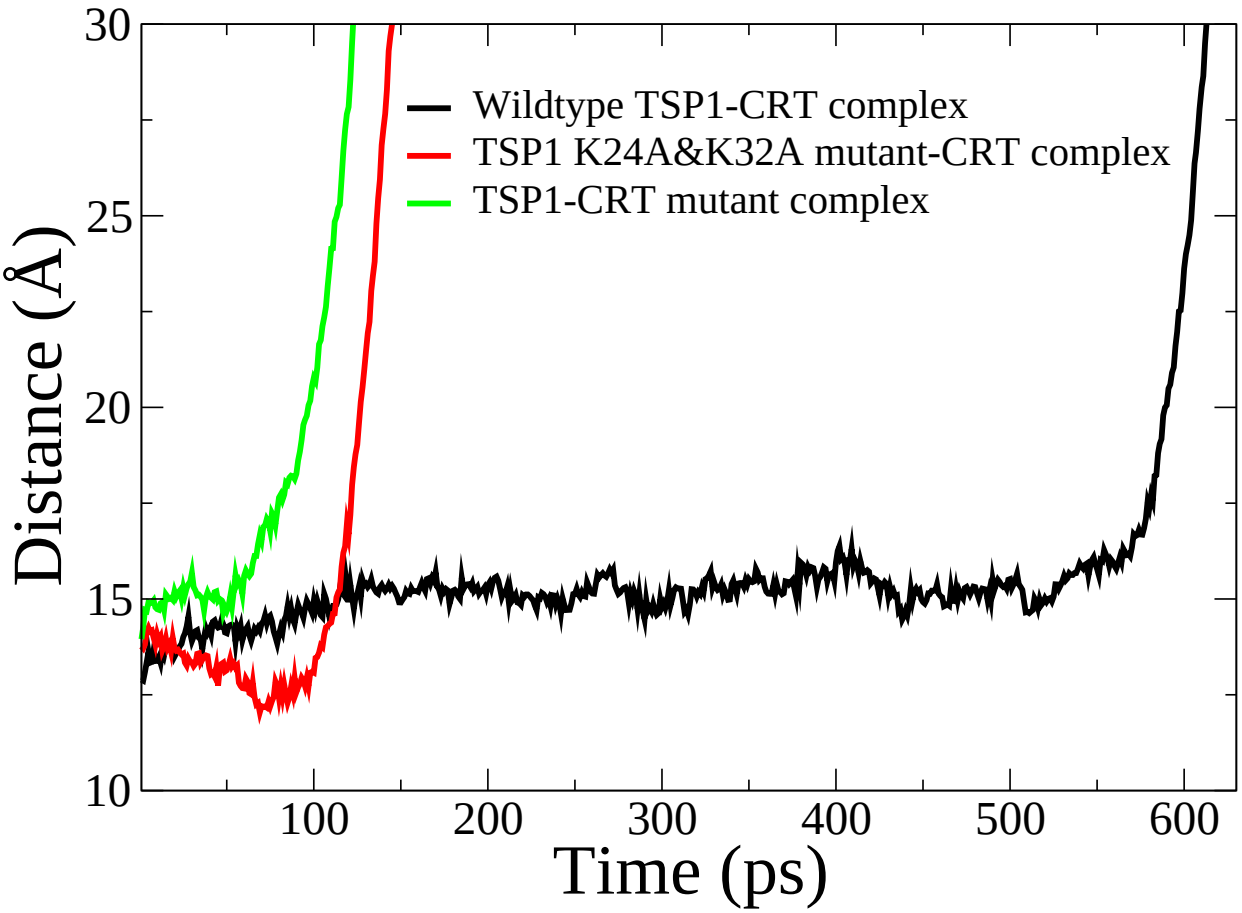

Figure 2S The distances between the centers of mass of the binding sites for wildtype TSP1-CRT complex, TSP1 K24A&K32A mutant-CRT complex and TSP1-CRT mutant under the constant force SMD simulations.

RMSD of TSP1 and its mutant

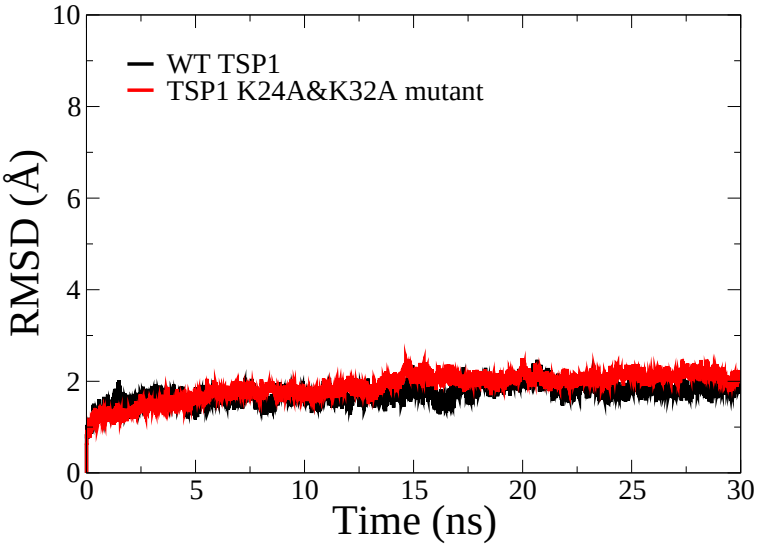

Figure 3S RMSD for TSP1-N domain over the 30ns MD simulation.

RMSD of CRT a

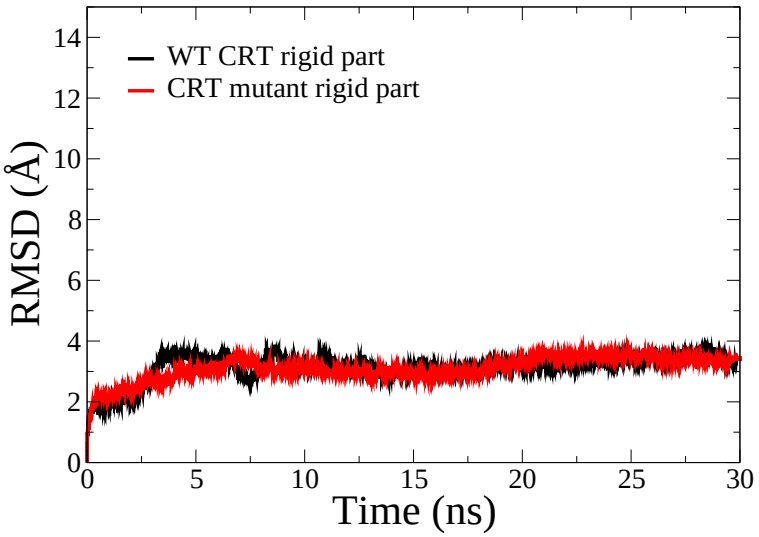

Figure 4S RMSD for CRT N-domain and the partial C-domain over the 30ns MD simulation

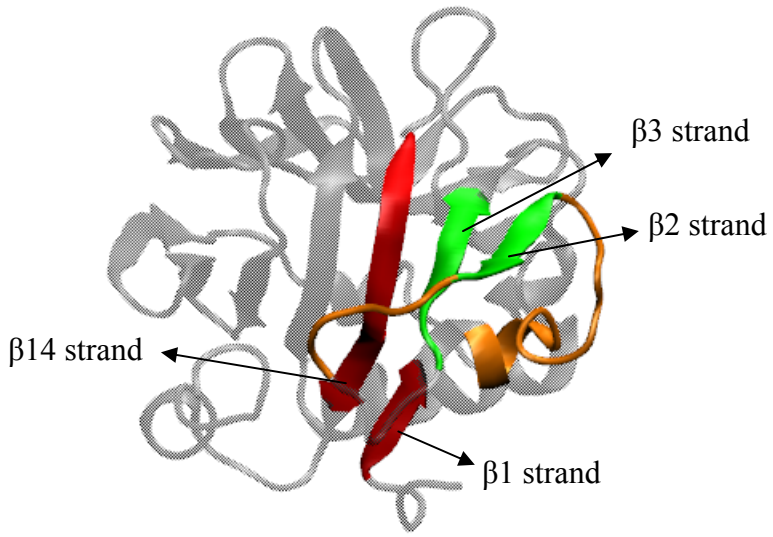

Figure 5S. TSP1 N-domain structure . Orange: CRT binding site in TSP1 (residues 17-35); green: β2 and β3 strands; red: β1 and β14 strands; grey: regions of TSP1 N-domain except CRT binding site in TSP1, β1, β2, β3 and β14 strands.

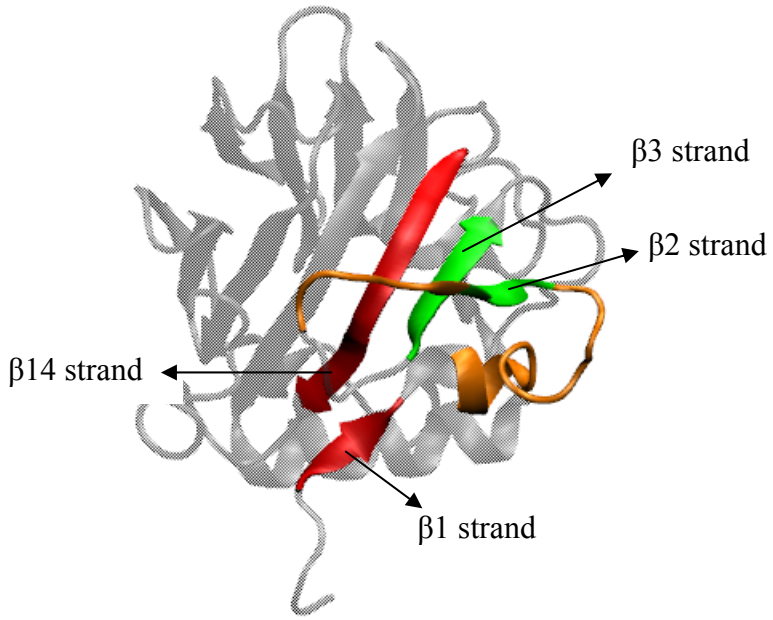

Figure 6S. Structure of TSP1 N-domain K24A & K32A mutant. Orange: CRT binding site in TSP1 (residues 17-35); green: β2 and β3 strands; red: β1 and β14 strands; grey: regions of TSP1 N-domain except CRT binding site in TSP1, β1, β2, β3 and β14 strands.

Table 1S Occupancy of the hydrogen bond formed between residues in the β strands of TSP1 and its mutant over the last 20ns MD simulation trajectories.

		Wildtype TSP1		TSP1 K24A&K32A mutant	
		donor-acceptor		donor-acceptor	
β1-β14	F13-F199	83.6%		F13-F199	74.9%
	F199-F13	82.8%		F199-F13	87.8%
	I15-V197	87.4%		I15-V197	39.1%
β2-β3	V31-A40	88.5%		V31-A40	89.0%
	R29-R42	59.6%		R29-R42	67.2%
	R42-R29	74.2%		R42-R29	76.9%
	E44-G27	67.8%		E44-G27	5.4%
β5-β10	L76-K136	92.8%		L76-K136	93.3%
	K136-L76	79.1%		K136-L76	85.3%
	L72-L140	85.2%		L72-L140	71.1%
	L140-L72	81.8%		L140-L72	71.1%
	A74-I138	76.4%		A74-I138	82.0%
	I138-A74	89.2%		I138-A74	91.7%
	F70-V142	62.7%		F70-V142	53.6%
	V142-F70	83.8%		V142-F70	83.2%
β5-β14	L73-R198	87.4%		L73-R198	91.8%
	R198-L73	80.2%		R198-L73	84.4%
	R77-V193	75.4%		R77-V193	79.5%
	V193-R77	84.2%		V193-R77	89.1%
β6-β7	L87-V101	88.9 %		L87-V101	86.0 %
	V101-L87	54.5%		V101-L87	62.0%

	L89-F99	67.6%	L89-F99	54.8%
	F99-L89	72.5%	F99-L89	27.4%
β6-β13	A88-R180	91.3%	A88-R180	77.4%
	R180-A88	89.9%	R180-A88	89.2%
β7-β8	V102-D111	90.8%	V102-D111	87.9%
	D111-V102	72.1%	D111-V102	65.6%
	N104-T109	82.3%	N104-T109	80.1%
	T109-N104	41.6%	T109-N104	51.2%
	S100-S113	68.6%	S100-S113	73.5%
	S113-S100	77.4%	S113-S100	49.3%
β8-β9	L110-V125	81.9%	L110-V125	76.2%
	V125-L110	79.4%	V125-L110	77.1%
	L112-V123	72.4%	L112-V123	68.4%
	V123-L112	77.3%	V123-L112	52.0%
β10-β11	Q143-R146	66.1%	Q143-R146	88.6%
	R146-Q143	67.4%	R146-Q143	61.6%
	T139-Y150	80.3%	T139-Y150	78.4%
	Y150-T139	63.2%	Y150-T139	67.5%
	F141-Q148	82.8%	F141-Q148	84.9%
	Q148-F141	84.1%	Q148-F141	77.6%
β11-β12	L149-E157	86.2%	L149-E157	87.8%
	E157-L149	60.6%	E157-L149	74.1%
	A147-A159	83.9%	A147-A159	82.9%
	A159-A147	53.8%	A159-A147	61.6%

	I151-K155	78.6%	I151-K155	87.8%
	K155-I151	68.9%	K155-I151	71.2%

Table 2S Occupancy of the hydrogen bond formed between residues in the β strands of CRT and its mutant over the last 20ns MD simulation trajectories.

		Wildtype CRT	CRT mutant (res 24-26&32-34 mutated to Ala)	
	donor-acceptor		donor-acceptor	
β2-β3	V33-Q50	89.5%	A33-Q50	0.0%
	Q50-V33	81.1%	Q50-A33	0.1%
	S35-G48	80.5%	S35-G48	75.9%
	G48-S35	82.8%	G48-S35	59.2%
β5-β12	L74-V159	79.3%	L74-V159	72.5%
	V159-L74	90.8%	V159-L74	87.7%
	V76-L157	84.8%	V76-L157	93.7%
	L157-V76	87.8%	L157-V76	94.2%
β6-β8	G89-I119	79.1%	G89-I119	0.0%
	I119-G89	0.0%	I119-G89	77.0%
β7-β8	V93-F115	68.7%	V93-F115	90.1%
	F115-V93	72.4%	F115-V93	87.8%
	L95-I113	68.6%	L95-I113	73.8%
	I113-L95	87.2%	I113-L95	85.5%
β8-β9	M114-I130	52.0%	M114-I130	74.3%

	I130-M114	67.2%	I130-M114	83.1%
	G116-H128	78.7%	G116-H128	73.9%
	H128-G116	83.4%	H128-G116	84.5%
B9-β10	F131-I144	91.9%	F131-I144	90.9%
	I144-F131	85.8%	I144-F131	77.9%
	Y133-K142	55.2%	Y133-K142	86.0%
	K142-Y133	81.1%	K142-Y133	85.8%
	C146-V129	85.2%	C146-V129	76.9%
β11-β12	T156-K168	41.4%	T156-K168	75.5%
	K168-T156	93.0%	K168-T156	87.4%
	I158-E166	76.7%	I158-E166	61.7%
	E166-I158	87.9%	E166-I158	76.7%
β12-β13	Y165-G177	83.8%	Y165-G177	86.1%
	G177-Y165	76.1%	G177-Y165	71.4%
	V167-E175	66.6%	V167-E175	69.4%
	E175-V167	74.3%	E175-V167	53.5%
	I169-S172	87.3%	I169-S172	82.4%
	S172-I169	73.2%	S172-I169	82.0%
	V174-V167	92.1%	V174-V167	67.8%